Inorg. Chem. **2003**, *42*, 3274–3284

Silylene-Bridged Dinuclear Iron Complexes $[Cp(OC)_2Fe]_2SiX_2$ (X = H, F, Cl, Br, I). Synthesis, Molecular Structure, Vibrational Spectroscopy, and Theoretical Studies†

Matthias Vögler,‡ Ioana Pavel,§ Marco Hofmann,‡ Damien Moigno,§ Martin Nieger,# Wolfgang Kiefer,*,§ and Wolfgang Malisch*,‡

Institut für Anorganische Chemie der Universität Würzburg, Institut für Physikalische Chemie der Universität Würzburg, Am Hubland, D-97074 Würzburg, Germany, and Institut für Anorganische Chemie der Universität Bonn, Gerhard-Domagk-Strausse 1, D-53121 Bonn, Germany

Received October 29, 2002

The μ_2-silylene-bridged iron complexes $[Cp(OC)_2Fe]_2SiX_2$ (X = F (**2**), Br (**4**), I (**5**)) have been prepared from the μ_2-SiH_2 functional precursor $[Cp(OC)_2Fe]_2SiH_2$ (**1**) by hydrogen/halogen exchange, using HBF_4, CBr_4, and CH_2I_2, respectively. The fluoro- and bromo-substituted derivatives **2** and **4** are converted upon UV irradiation to the carbonyl- and dihalosilylene-bridged dinuclear complexes $[Cp(OC)Fe]_2(\mu_2\text{-CO})(\mu_2\text{-}SiX_2)$ (X = F (**6**), Br (**7**)) via CO elimination. All new compounds have been characterized spectroscopically, and, in addition, the molecular structure of **2**, **4**, and the previously reported chloro derivative $[Cp(OC)_2Fe]_2SiCl_2$ (**3**) has been determined by single-crystal X-ray diffraction methods. For **1**–**5**, the Fourier transform infrared and Raman spectra have been recorded and discussed, together with density functional theory calculations, which support the experimental results of the structural and vibrational analysis. The computed geometries, harmonic vibrational wavenumbers, and their corresponding Raman scattering activities are in good agreement with the experimental data. A significant dependence of the CO and Fe–Si stretching modes on the X substituents of the μ_2-silylene bridge has been observed and discussed.

Introduction

The chemistry of transition-metal silicon compounds has been an active field of research ever since the early works of Chalk and Harrod[1] on the transition-metal-catalyzed hydrosilylation of olefins. In the past decades, a huge number of silyl complexes of almost all transition metals have been synthesized and characterized.[2] Especially, some palladium and platinum derivatives are encountered as crucial intermediates, not only in hydrosilylation reactions[3] but also in other catalytic processes (e.g., dehydrogenative coupling of SiH moieties[4]) or in ring-opening methatesis polymerization (ROMP) reactions of cyclic disilanes.[5]

A central issue in understanding the mechanistic details of these catalytic processes is the strength of the metal−silicon bond. Some insight can be gained from structural data that are available for many transition-metal silyl complexes. For example, the bond lengths observed in $H_3Si-Co(CO)_4$ (2.381 Å)[6] and $F_3Si-Co(CO)_4$ (2.226 Å)[7] indicate that the

* Authors to whom correspondence should be addressed. E-mail address (W.M.): Wolfgang.Malisch@mail.uni-wuerzburg.de. Fax: +49 931 888 4618.

† Part 59 of the series "Synthesis and Reactivity of Silicon Transition Metal Complexes". For part 58, see: Malisch, W.; Jehle, H.; Schumacher, D.; Binnewies, M.; Söger, N. *J. Organomet. Chem.* **2003**, *667*, 35-41.

‡ Institut für Anorganische Chemie der Universität Würzburg.

§ Institut für Physikalische Chemie.

Institut für Anorganische Chemie der Universität Bonn.

(1) (a) Chalk, A. J.; Harrod, J. F. *J. Am. Chem. Soc.* **1965**, *87*, 1133−1135. (b) Chalk, A. J.; Harrod, J. F. *J. Am. Chem. Soc.* **1967**, *89*, 1640−1647.

(2) (a) Corey, J. Y.; Braddock-Wilking, J. *Chem. Rev.* **1999**, *99*, 175−292. (b) Braunstein, P.; Knorr, M. *J. Organomet. Chem.* **1995**, *500*, 21−38. (c) Zybill, C.; Handwerker, H.; Friedrich, H. *Adv. Organomet. Chem*. **1994**, *36*, 229−281. (d) Tilley, T. D. In *Transition Metal Silyl Derivatives*; Patai, S., Rappoport, Z., Eds.; Wiley: New York, 1991; p 245. (e) Cundy, C. S.; Kingston, B. M.; Lappert, M. F. *Adv. Organomet. Chem*. **1973**, *11*, 253−330. (f) Schubert, U. *Adv. Organomet. Chem.* **1990**, *30*, 151−187. (g) Aylett, B. J. *Adv. Inorg. Chem. Radiochem*. **1982**, *25*, 1−133. (h) Malisch, W.; Kuhn, M. *Chem. Ber*. **1974**, *107*, 979−995.

(3) (a) Speier, J. L. *Adv. Organomet. Chem*. **1979**, 407−447. (b) Ojima, I. In *The Chemistry of Organic Silicon Compounds*; Patai, S., Rappoport, Z., Eds.; Wiley: Chichester, U.K., 1989; p 1479. (c) Chalk, A. J.; Harrod, J. F. *J. Am. Chem. Soc.* **1965**, *87*, 16−21.

(4) (a) Yamashita, M.; Tanaka, M. *Bull. Chem. Soc. Jpn*. **1995**, *68*, 403−419. (b) Tilley, T. D. *Acc. Chem. Res.* **1993**, *26*, 22−29. (c) Hengge, E. In *Organosilicon Chemistry*; Auner, N., Weis, J., Eds.; Wiley−VCH: Weinheim, Germany, 1994; p 275.

(5) (a) Uchimaru, Y.; Tanaka, Y.; Tanaka, M. *Chem. Lett*. **1995**, 164. (b) Recatto, C. A. *Aldrichimica Acta* **1995**, *28*, 85−92.

(6) Aylett, B. J. *Adv. Inorg. Chem. Radiochem*. **1968**, *11*, 249−307.

10.1021/ic026138v CCC: $25.00
Published on Web 04/16/2003

presence of electronegative substituents on the Si atom can greatly increase the strength of the metal−silicon bond. The M−Si bond distances in many structurally characterized silyl complexes L_nM-SiR_3 (M = Mn, Fe, Co, Rh, Pt) were found to be up to 0.28 Å shorter than those that would be predicted on the basis of the covalent atom radii.[2e] These short bond distances are generally attributed to a π-type back-bonding from the d-orbitals of the transition metal into the antibonding σ^*(Si−R) orbitals of the silyl group $-SiR_3$.[8] Consequently, the M−Si bonds in silyl complexes of d^0 metals (Ti^{IV}, Zr^{IV}) show no significant shortening and closely match the predicted covalent values.[9] In the Mössbauer and IR spectral investigations of Pannell et al. on $Cp(OC)_2Fe-R$ (where R represents a large range of alkyl and silyl groups), the increase in s-electron density at the metal center for the silyl compounds has been attributed to a superior σ-donation from the silyl group, as compared with the alkyl group, rather than to significant iron−silicon π-type back-bonding.[10] Important π-type back-bonding effects were only observed for the $Cp(OC)_2Fe-SiMe_{3-n}Ph_n$ complexes. However, valence photoelectron spectra that were recorded by Lichtenberger and Rai-Chaudhuri for the complexes $Cp(OC)_2Fe-SiR_3$ (R = Me, Cl) have confirmed that silyl substituents can act as effective π-acceptors.[11] In a more recent structural and theoretical study on a series of osmium complexes $(Ph_3P)_2(OC)(Cl)Os-SiR_3$ (R = F, Cl, OH, Me), Roper et al. examined the ionic and covalent contributions to the metal−silicon bond in detail.[8a]

We have now prepared five homologous complexes of the general formula $[Cp(OC)_2Fe]_2SiX_2$ (X = H (**1**), F (**2**), Cl (**3**), Br (**4**), I (**5**)) with the original intention of using these compounds as precursors for the synthesis of the bis(metallo)silanediol $[Cp(OC)_2Fe]_2Si(OH)_2$[12a] or the bis(metallo)silylene $[Cp(OC)_2Fe]_2Si$. Furthermore, the availability of this series of compounds gave us the opportunity to study, in detail, the bonding situation in bismetalated silanes, which are among a class of compounds for which a growing number of representatives has been prepared in recent years.[12] In this sense, the experimental research and development has demonstrated vibrational spectroscopy to be one of the most useful tools for obtaining information about the strength of the bonds in a molecule, even though the direct assignment of observed IR and Raman bands of comparatively complex molecules is fraught with problems. Theoretical calculations can certainly assist in obtaining a deeper understanding of vibrational spectra of larger organometallic arrangements, such as transition-metal silyl complexes. In particular, recent developments in density functional theory (DFT) have shown that DFT may become a powerful computational alternative to the conventional quantum chemical methods, because DFT methods are far less computationally demanding and take account of the effects of electron correlation.[13,14] Methods based on DFT were successfully used recently to predict the structural properties and the Raman vibrational modes of new transition-metal complexes accurately.[15,16] Thus, to complete the previous characterization of $[Cp(OC)_2Fe]_2SiH_2$ (**1**)[12b,i] and to obtain a better understanding of the influence of a wide range of SiX_2 groups on the nature of the Fe−Si and CO bonds, Fourier transform infrared and Raman (FT−Raman) spectra of complexes **1**−**5** were recorded for the first time and discussed in combination with the results of our DFT calculations.

Experimental Section

General. All manipulations were performed in an inert atmosphere of purified and dried nitrogen, using standard Schlenk techniques. Solvents were appropriately dried and purified, using standard procedures. NMR spectra were recorded at room temperature on a JEOL model JNM-LA 300 spectrometer. All chemical shifts are in parts per million (ppm) and have been referenced to solvent signals (^{1}H and ^{13}C) or to the external standards H_3PO_4 (^{31}P) and trimethylsilane (TMS) (^{29}Si). IR spectra were recorded using a Perkin−Elmer model 283 spectrophotometer. Samples were prepared as solutions in a NaCl cell. $[Cp(OC)_2Fe]_2SiH_2$ (**1**)[12b] and $[Cp(OC)_2Fe]_2SiCl_2$ (**3**)[12c] were obtained according to literature procedures.

$[Cp(OC)_2Fe]_2SiF_2$ (2). A solution of $[Cp(OC)_2Fe]_2SiH_2$ (**1**) (280 mg, 0.73 mmol) in benzene (15 mL) was treated at 5 °C with a solution of HBF_4 (128 mg, 1.46 mmol) in diethyl ether (10 mL). While the solution was stirred, gas evolution (BF_3, H_2) was observed, and the gas was removed from the reaction vessel in a continuous stream of nitrogen. After 1 h, the solution was filtered through a pad of Celite and condensed in vacuo to 1 mL. Upon the addition of *n*-pentane (5 mL), a light-yellow solid of **2** precipitated, which was filtered from the solution, washed twice with *n*-pentane (each 3 mL), and dried in vacuo. Yield: 150 mg (50%). Light-yellow solid; mp: 178 °C. ^{1}H NMR (300.4 MHz, C_6D_6): δ = 4.28 ppm (s, H_5C_5). ^{13}C{^{1}H} NMR (75.5 MHz, C_6D_6): δ = 84.1 (s, C_5H_5), 214.5 ppm (s, CO). ^{19}F{^{1}H} NMR (376.5 MHz, C_6D_6): δ = −36.6 ppm (s, $^1J_{SiF}$ = 437 Hz). ^{29}Si{^{1}H} NMR (59.6 MHz, C_6D_6): δ = 109.4 ppm (t, $^1J_{SiF}$ = 437 Hz). Anal. Calcd for $C_{14}H_{10}F_2Fe_2O_4Si$ (420.01): C, 40.04; H, 2.40. Found: C, 39.54; H, 2.63.

(7) Archer, N. J.; Haszeldine, R. N.; Parish, R. V. *Chem. Commun*. **1971**, 524−525.

(8) (a) Hübler, K.; Hunt, P. A.; Maddock, S. M.; Rickard, C. E. F.; Roper, W. R.; Salter, D. M.; Schwerdtfeger, P.; Wright, L. J. *Organometallics* **1997**, *16*, 5076−5083. (b) Lemke, F. R.; Galat, K. J.; Youngs, W. J. *Organometallics* **1999**, *18*, 1419−1429. (c) Freeman, S. T. N.; Lofton, L. L.; Lemke, F. R. *Organometallics* **2002**, *21*, 4776−4784.

(9) Muir, K. W. *J. Chem. Soc. A* **1971**, 2663−2666.

(10) Pannell, K. H.; Wu, C. C.; Long G. J. *J. Organomet. Chem.* **1980**, *186*, 85−90.

(11) Lichtenberger, D. L.; Rai-Chaudhuri, A. *J. Am. Chem. Soc.* **1991**, *113*, 2923−2930.

(12) (a) Malisch, W.; Vögler, M.; Schumacher, D.; Nieger, M. *Organometallics* **2002**, *21*, 2891−2897. (b) Malisch, W.; Vögler, M.; Käb, H.; Wekel, H.-U. *Organometallics* **2002**, *21*, 2830−2832. (c) Malisch, W.; Ries, W. *Chem. Ber.* **1979**, *112*, 1304−1315. (d) Malisch, W.; Ries, W. *Angew. Chem.* **1978**, *90*, 140−141; *Angew. Chem., Int. Ed. Engl*. **1978**, *17*, 120−121. (e) Ogino, H.; Tobita, H. *Adv. Organomet. Chem.* **1998**, *42*, 223−290. (f) Luh, L. S.; Wen, Y. S.; Tobita, H.; Ogino, H. *Bull. Chem. Soc. Jpn*. **1997**, *70*, 2193−2200. (g) Pannell, K. H.; Sharma, H. *Organometallics* **1991**, *10*, 954−959. (h) Ueno, K.; Hamashima, N.; Shimoi, M.; Ogino, H. *Organometallics* **1991**, *10*, 959−962. (i) Aylett, B. J.; Colquhoun, H. M. *J. Chem. Res. Synop.* **1977**, *1*, 148.

(13) Parr, R. G.; Yang, W. *Density Functional Theory of Atoms and Molecules*; Oxford University Press: Oxford, U.K., 1989.

(14) Seminario, J. M.; Politzer, P. *Modern Density Functional Theory, A Tool for Chemistry*; Elsevier Science B. V.: Amsterdam, The Netherlands, 1995.

(15) (a) Berces, A.; Ziegler, T. *J. Phys. Chem.* **1994**, *98*, 13233−13242. (b) Berces, A.; Ziegler, T. *Top. Curr. Chem.* **1996**, *182*, 41−85.

(16) (a) Jonas, V.; Thiel, W. *J. Phys. Chem.* **1995**, *99*, 8474−8484. (b) Jonas, V.; Thiel, W. *J. Phys. Chem.* **1996**, *100*, 3636−3648.

Table 1. Crystallographic Data for Compounds **2**−**4**

	$[Cp(OC)_2Fe]_2SiF_2$ (**2**)	$[Cp(OC)_2Fe]_2SiCl_2$ (**3**)	$[Cp(OC)_2Fe]_2SiBr_2$ (**4**)
empirical formula	$C_{14}H_{10}F_2Fe_2O_4Si$	$C_{14}H_{10}Cl_2Fe_2O_4Si$	$C_{14}H_{10}Br_2Fe_2O_4Si$
fw	420.01	452.91	541.83
temp	123 ± 2 K	123 ± 2 K	123 ± 2 K
wavelength (Mo Kα)	0.71073 Å	0.71073 Å	0.71073 Å
cryst syst	monoclinic	monoclinic	monoclinic
space group	*P*2(1)/*n* (No. 14)	*C*2/*c* (No. 15)	*C*2/*c* (No. 15)
unit cell dimensions			
a	7.7190(1) Å	19.0362(6) Å	16.429(4) Å
b	16.9176(2) Å	7.4253(3) Å	7.624(2) Å
c	11.6193(2) Å	13.5488(4) Å	14.816(4) Å
α	90°	90°	90°
β	98.500(1)°	*β* = 120.102(2)°	116.91(2)°
γ	90°	90°	90°
vol (Å^3)	1500.66(4) Å^3	1656.83(10) Å^3	1654.8(7) Å^3
Z	4	4	4
calculated density	1.859 Mg/m^3	1.816 Mg/m^3	2.175 Mg/m^3
abs coeff	2.050 mm^{-1}	2.159 mm^{-1}	6.668 mm^{-1}
F(000)	840	904	1048
cryst size	0.40 mm × 0.20 mm × 0.10 mm	0.25 mm × 0.20 mm × 0.15 mm	0.25 mm × 0.08 mm × 0.02 mm
θ range	2.93° < *θ* < 25.00°	3.01° < *θ* < 28.29°	2.78° < *θ* < 25.00°
reflns (collected/unique)	28 456/2630	14 631/2047	6252/1455
R (int)	0.0488	0.0453	0.1629
absorption correction	empirical	empirical	empirical
GOF on F^2	1.037	1.078	0.983
R1 [$I > 2\sigma(I)$]	0.0164	0.0226	0.0597
wR2 (all data)	0.0436	0.0578	0.1326
largest diff. peak and hole	0.246, −0.249 e/Å^3	0.356, −0.355 e/Å^3	0.829, −1.054 e/Å^3

$[Cp(OC)_2Fe]_2SiBr_2$ (4). Tetrabromomethane (180 mg, 0.54 mmol) was added at room temperature to a solution of $[Cp(OC)_2Fe]_2SiH_2$ (**1**) (188 mg, 0.49 mmol) in benzene (10 mL). After the solution was stirred for 1 h, all volatiles were removed in vacuo and the remaining yellow-orange residue of **4** was washed twice with 5 mL of cold *n*-pentane and dried in vacuo. Yield: 240 mg (93%). Yellow-orange solid; mp: 45 °C (dec.). ^{1}H NMR (300.4 MHz, C_6D_6): δ = 4.28 ppm (s, H_5C_5). ^{13}C{^{1}H} NMR (75.5 MHz, C_6D_6): δ = 86.8 (s, C_5H_5), 214.7 ppm (s, CO). ^{29}Si{^{1}H} NMR (59.6 MHz, C_6D_6): δ = 141.4 ppm (s). Anal. Calcd for $C_{14}H_{10}Br_2Fe_2O_4Si$ (541.83): C, 31.03; H, 1.86. Found: C, 30.76; H, 2.04.

$[Cp(OC)_2Fe]_2SiI_2$ (5). A solution of $[Cp(OC)_2Fe]_2SiH_2$ (**1**) (410 mg, 1.07 mmol) in 10 mL of benzene was treated with an excess of CH_2I_2 (2.70 g, 10.1 mmol). After the solution was stirred for 8 h at 50 °C, all volatiles were removed in vacuo and the remaining residue of **5** was washed twice with cold *n*-pentane (each 5 mL) and then dried in vacuo. Yield: 598 mg (88%). Yellow solid; mp: 92 °C (dec.). ^{1}H NMR (300.4 MHz, C_6D_6): δ = 4.27 (s, H_5C_5). ^{13}C{^{1}H} NMR (75.5 MHz, C_6D_6): δ = 88.2 (s, C_5H_5), 215.7 ppm (s, CO). ^{29}Si{^{1}H} NMR (59.6 MHz, C_6D_6): δ = 105.0 ppm (s). Anal. Calcd for $C_{14}H_{10}Fe_2I_2O_4Si$ (635.81): C, 26.45; H, 1.59. Found: C, 26.71; H, 1.84.

$[Cp(OC)Fe]_2Si(\mu\text{-}CO)(\mu\text{-}SiF_2)$ (6). A solution of $[Cp(OC)_2Fe]_2SiF_2$ (**2**) (69 mg, 0.16 mmol) in 3 mL of benzene was irradiated with UV light (quartz lamp model TQ 150, 150 W, Hanau) and the reaction mixture was monitored by ^{1}H NMR. After 0.5 h, all insoluble material was removed by filtration through a pad of Celite and the filtrate was condensed in vacuo to 1 mL. A dark-red solid of **6** precipitated when 2 mL of cold *n*-pentane was added; this precipitate was filtered from the solution, washed twice with *n*-pentane (each 0.5 mL), and dried in vacuo. Yield: 35 mg (54%). Dark-red solid; mp: 148 °C. IR (cyclohexane): ν(CO) = 2031(m), 1999 (w), 1988 (s), 1961 (vs); 1794 (vs) cm^{-1}. Cis-isomer (**6a**): ^{1}H NMR (100 MHz, C_6H_6): δ = 4.13 ppm (s, H_5C_5). ^{19}F{^{1}H} NMR (94.1 MHz, C_6H_6): δ = 57.0 (d, $^2J_{FSiF}$ = 85.1 Hz), 59.6 ppm (d, $^2J_{FSiF}$ = 85.1 Hz). Trans-isomer (**6b**): ^{1}H NMR (100 MHz, C_6H_6): δ = 4.33 ppm (s, H_5C_5). ^{19}F{^{1}H} NMR (94.1 MHz, C_6H_6): δ = 58.1 ppm (s). Anal. Calcd for $C_{13}H_{10}F_2Fe_2O_3Si$ (392.00): C, 39.83; H, 2.57. Found: C, 39.41; H, 3.01.

$[Cp(OC)Fe]_2Si(\mu\text{-}CO)(\mu\text{-}SiBr_2)$ (7). Using a procedure similar to that used to synthesize **6**, $[Cp(OC)_2Fe]_2SiBr_2$ (**4**) (120 mg, 0.22 mmol) in 5 mL of benzene was irradiated with UV light (quartz lamp model TQ 718, 700 W, Hanau) for 3 h. A dark-red solid of **7** precipitated when 3 mL of cold *n*-pentane was added; this precipitate was filtered from the solution, washed twice with *n*-pentane (each 1 mL), and dried in vacuo. Yield: 88 mg (76%). Dark-red solid; IR (cyclohexane): ν(CO) = 1996 (vs), 1951 (s); 1787 (s) cm^{-1}. Cis-isomer (**7a**): ^{1}H NMR (300.4 MHz, C_6D_6): δ = 4.06 ppm (s, H_5C_5). ^{13}C{^{1}H} NMR (75.5 MHz, C_6D_6): δ = 86.8 (s, C_5H_5), 213.3 ppm (s, CO). ^{29}Si{^{1}H} NMR (59.6 MHz, C_6D_6): δ = 181.1 ppm (s). Trans-isomer (**7b**): ^{1}H NMR (300.4 MHz, C_6D_6): δ = 4.25 ppm (s, H_5C_5). ^{13}C{^{1}H} NMR (75.5 MHz, C_6D_6): δ = 87.7 (s, C_5H_5), 210.3 ppm (s, CO). Anal. Calcd for $C_{13}H_{10}Br_2Fe_2O_3Si$ (513.90): C, 30.39; H, 1.96. Found: C, 30.75; H, 2.48.

X-ray Crystal Structure Determination. Crystallographic data are summarized in Table 1. Suitable single crystals of **2**−**4** were obtained by the slow evaporation of a saturated solution of the respective compound in diethyl ether. The intensities were measured with a Nonius−Kappa CCD diffractometer (Mo Kα radiation, λ = 0.71073 Å; graphite monochromator) at T = 123 ± 2 K. The structure was solved by the Patterson method (SHELXS-97)[17a] and refined by least-squares methods based on F^2 with all measured reflections (SHELXL-97) (full-matrix least-squares on F^2).[17b] Non-hydrogen atoms were refined anisotropically; H atoms were calculated according to the ideal geometry. An empirical absorption correction was applied. Additional crystallographic data are given in the Supporting Information.

Computational Details. The DFT calculations were performed using the Gaussian 98 program package.[18] Becke's 1988 exchange

(17) (a) Sheldrick, G. M. *Acta Crystallogr., Sect. A: Found. Crystallogr.* **1990**, *A46*, 467−473. (b) Sheldrick, G. M. *SHELXL-97*; University of Göttingen: Göttingen, Germany, 1997.

functional,[19] in combination with the Perdew−Wang 91 correlation functional (BPW91),[20] was employed in the calculation. The 6-311G(d) Pople split valence basis set implemented in the Gaussian 98 program[18] was chosen in the geometry optimization and normal mode calculations of **1**−**4**, taking into account that results obtained with a split valence set are a significant improvement on those obtained with a minimal basis set.[21] Because of the presence of I atoms in complex **5**, the calculations were performed in this case using the 3-21G(d) basis set[18] for the I atoms and the 6-311G(d) basis set for the other atoms. DFT calculations on harmonic vibrational modes and Raman scattering activity of each band were performed using the fully optimized molecular geometry without symmetry restrictions, and the analytical harmonic vibrational wavenumbers for all structures confirmed that local minima on the potential energy surface had been found. The partial charges (given in units of e) situated on selected atoms of **1**−**5** were then determined by the natural population analysis (NPA)[22] at the same level of theory. To obtain further information regarding the electronic structures, NBO (natural bond orbital) analyses were also performed.[23−26] The essential feature of NBO analysis is that the electron density is represented, as far as possible, by localized core orbitals, bonds, and lone pairs. These orbitals comprise Lewis structures corresponding precisely to the chemist's view of molecules built from atoms connected by localized two-electron bonds. However, for conjugated systems, ideal Lewis structures are obviously not adequate. Deviations from idealized Lewis structures due to conjugation are shown in NBO analysis as orbital interactions between localized bonds and antibonds and between lone pairs and antibonds. The energetic contributions from these interactions can be quantified with the help of second-order perturbation theory.

Results and Discussion

I. Preparative Results. In the series of dihalosilylene-bridged dinuclear iron complexes $[Cp(OC)_2Fe]_2SiX_2$, only the fluoro- and chloro-substituted representatives **2** (X = F) and **3** (X = Cl) have been prepared until now via chlorination of $[Cp(OC)_2Fe]_2Si(Cl)H$ with CCl_4 to give **3**, which, on treatment with $AgBF_4$ at 70 °C, is transformed to **2**.[12c]

We now have found that the SiH_2-substituted bis(ferrio)-silane $[Cp(OC)_2Fe]_2SiH_2$ (**1**)[12b,i] is a valuable starting material for the generation of the fluoro-substituted derivatives, as well as for the generation of the yet unknown bromo- and iodo-substituted derivatives. This is due to the extreme activation of the Si−H functions by the two transition-metal fragments, with respect to Si−H/Si−Hal exchange, which can be deduced from the very low $\tilde{\nu}_{SiH}$ absorption (2037 cm^{-1}).[12b] This value is even ca. 55 cm^{-1} lower than that in $Cp(OC)_2Fe-SiH_3$ (2093 cm^{-1})[27] and indicates a very electron-rich SiH_2 unit for **1**.

Scheme 1

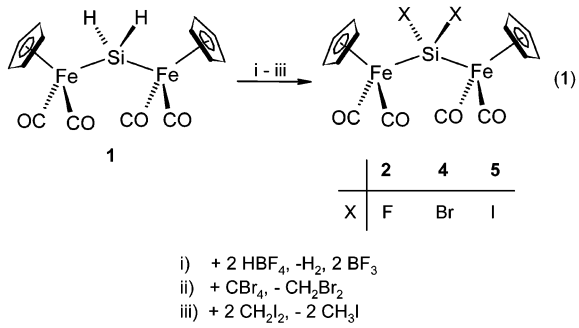

In this context, **2** is obtained by the fluorination of **1** at room temperature, using HBF_4 in diethyl ether. The reaction proceeds with the elimination of H_2 and BF_3 and produces $[Cp(OC)_2Fe]_2SiF_2$ (**2**) after 1 h in 50% yield (Scheme 1).

The dibromosilylene complex $[Cp(OC)_2Fe]_2SiBr_2$ (**4**) is generated from **1** after 1 h at room temperature, using a slight excess of tetrabromomethane in benzene. The formation of **4**, which can be isolated in excellent yield (93%), could be easily followed using IR and NMR spectroscopy by the disappearance of the SiH signals.

Attempts to generate $[Cp(OC)_2Fe]_2SiI_2$ (**5**) in an analogous manner, by treatment of **1** with CI_4, leads predominantly to the formation of $Cp(OC)_2Fe$-I by cleavage of the Fe−Si bond. However, when the milder iodination reagent CH_2I_2 was employed (in 10-fold excess at 50 °C), a controlled H/I exchange could be achieved, leading to **5** after 8 h in 88% yield.

Compounds **2**, **4**, and **5** are isolated as light-yellow (**2**, **5**) and yellow−orange (**4**) solids, which show good solubility in benzene, diethyl ether, and tetrahydrofuran. The ^{29}Si NMR spectra of **2**, **4**, and **5** clearly reveal the influence of two silicon-bonded $Cp(OC)_2Fe$ fragments. The paramagnetic term of the metal fragments leads to ^{29}Si NMR resonances downfield of 100 ppm in the following order of decreasing ppm values: **3** (146.2, X = Cl) > **4** (141.2, X = Br) > **2** (109.4, X = F) > **5** (105.0, X = I).

A characteristic feature of the dihalosilylene complexes **2**−**5** is their extreme sensitivity toward light. When **2** and **3** are exposed to light, slow decomposition is observed, leading predominantly to $[Cp(OC)_2Fe]_2$ with extrusion of the silylene "SiX_2" (X = F, Cl), giving rise to the formation of an insoluble product.[28] For **4** and **5**, the major decomposition product is $Cp(OC)_2Fe$-X (X = Br, I), as a result of the relatively weak Si−Br and Si−I bonds (343 and 339 kJ/mol, respectively).[29]

(18) Frisch, M. J.; Trucks, G. W.; Schlegel, H. B.; Scuseria, G. E.; Robb, M. A.; Cheeseman, J. R.; Zakrzewski, V. G.; Montgomery, J. A., Jr.; Stratmann, R. E.; Burant, J. C.; Dapprich, S.; Millam, J. M.; Daniels, A. D.; Kudin, K. N.; Strain, M. C.; Farkas, O.; Tomasi, J.; Barone, V.; Cossi, M.; Cammi, R.; Mennucci, B.; Pomelli, C.; Adamo, C.; Clifford, S.; Ochterski, J.; Petersson, G. A.; Ayala, P. Y.; Cui, Q.; Morokuma, K.; Malick, D. K.; Rabuck, A. D.; Raghavachari, K.; Foresman, J. B.; Cioslowski, J.; Ortiz, J. V.; Stefanov, B. B.; Liu, G.; Liashenko, A.; Piskorz, P.; Komaromi, I.; Gomperts, R.; Martin, R. L.; Fox, D. J.; Keith, T.; Al-Laham, M. A.; Peng, C. Y.; Nanayakkara, A.; Gonzalez, C.; Challacombe, M.; Gill, P. M. W.; Johnson, B. G.; Chen, W.; Wong, M. W.; Andres, J. L.; Head-Gordon, M.; Replogle, E. S.; Pople, J. A. *Gaussian 98*, revision A.7; Gaussian, Inc.: Pittsburgh, PA, 1998.
(19) Becke, A. D. *Phys. Rev. A* **1988**, *38*, 3098−3100.
(20) Perdew, J. P.; Wang, Y. *Phys. Rev. B* **1992**, *B45*, 13244−13249.
(21) Yamguchi, Y.; Frisch, M. J.; Gaw, J.; Schaefer, H. F.; Binkley, S. *J. Chem. Phys.* **1986**, *84*, 2262−2278.
(22) Reed, A. E.; Weinstock, R. B.; Weinhold, F. *J. Chem. Phys.* **1985**, *83*, 735−746.
(23) Reed, A. E.; Curtiss, L. A.; Weinhold, F. *Chem. Rev.* **1988**, *88*, 899−926.
(24) Foster, J. P.; Weinhold, F. *J. Am. Chem. Soc.* **1980**, *102*, 7211−7218.
(25) Reed, A. E.; Weinhold, F. *J. Chem. Phys.* **1985**, *83*, 1736−1740.
(26) Salzner, U.; Kiziltepe, T. *J. Org. Chem.* **1999**, *64*, 764−769.
(27) Malisch, W.; Möller, S.; Fey, O.; Wekel, H.-U.; Pikl, R.; Posset, U.; Kiefer, W. *J. Organomet. Chem.* **1996**, *507*, 117−124.

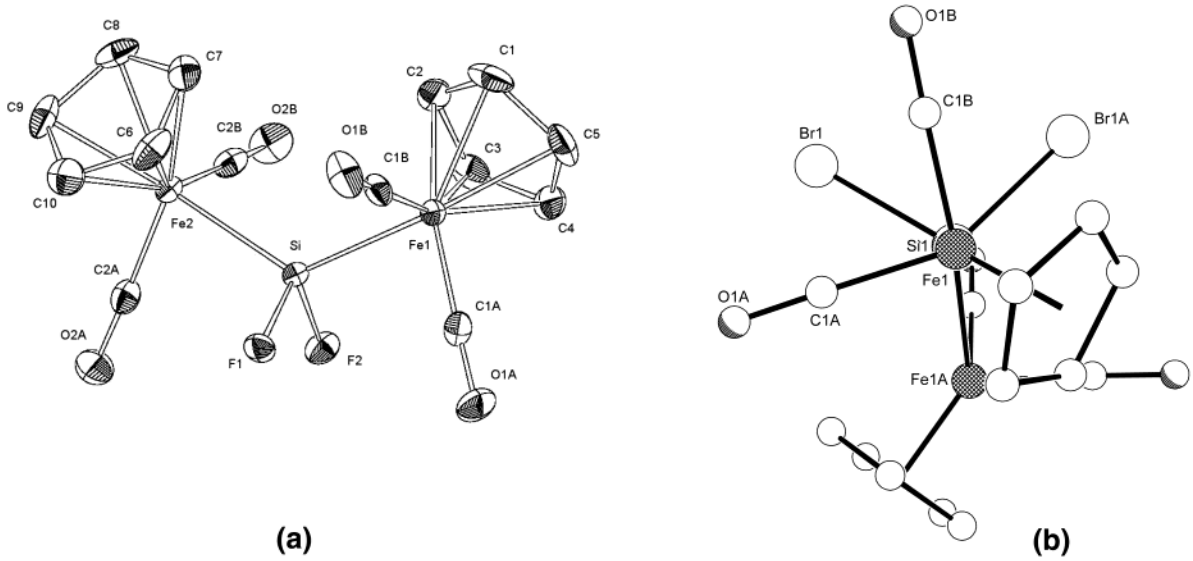

Figure 1. (a) ORTEP view of $[Cp(OC)_2Fe]_2SiF_2$ (**2**). Ellipsoids are at the 50% probability level. (b) View along the Fe1−Si1 axis of $[Cp(OC)_2Fe]_2SiBr_2$ (**4**).

Scheme 2

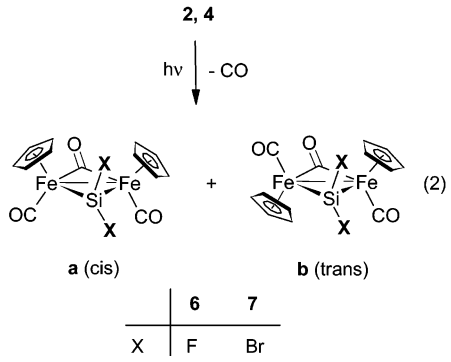

We also performed controlled UV irradiation experiments of **2**, **4**, and **5**, to determine if a cyclization process under CO elimination is possible, analogous to the formation of $[Cp(OC)Fe]_2(\mu_2\text{-}SiH_2)(\mu_2\text{-}CO)$ from **1**[12b] or $[Cp(OC)Fe]_2[\mu_2\text{-}Si(Me)(SiMe_3)](\mu_2\text{-}CO)$ from $[Cp(OC)_2Fe\text{-}SiMe_2]_2$.[12g,h] Indeed, in the case of the difluoro derivative **2**, a mixture of the CO-bridged complex $[Cp(OC)Fe]_2(\mu_2\text{-}SiF_2)(\mu_2\text{-}CO)$ (**6**), $[Cp(OC)_2Fe]_2$, and other byproducts is formed after UV irradiation for 0.5 h in benzene; from this mixture, **6** can be isolated, in 54% yield, as a dark-red solid (Scheme 2).

Irradiation of the dibromosilylene complex **4** in benzene proceeds more selectively and, after 3 h, leads to the formation of **7**, which is isolated, after removal of the byproduct $Cp(OC)_2Fe\text{-}Br$, in a yield of 76%. Compounds **6** and **7** form mixtures of cis-(**6a**/**7a**) and trans-(**6b**/**7b**) isomers, with the cis-isomer presumably dominating in both cases, as previously observed for **1**.[12b] Isomer ratios (cis:trans) of 57:43 (**6**) and 89:11 (**7**), respectively, can be determined from the intensity of the two Cp signals in the ^1H NMR spectrum. Moreover, in the case of **6**, a $^{19}F\{^1H\}$ NMR spectrum clearly proves the stereochemistry, with the cis-isomer showing an AB spectrum with resonances at 57.0 and 59.6 ppm ($^2J_{FSiF}$ = 85.1 Hz), and the trans-isomer showing a singlet at 58.1 ppm.

UV irradiation of the iodo derivative **5** does not lead to the formation of a μ-CO-bridged diiodo iron complex that is analogous to **6** and **7**. In this case, only the decomposition product $Cp(OC)_2Fe\text{-}I$ is formed almost quantitatively.

II. X-ray Analyses of $[Cp(OC)_2Fe]_2SiX_2$ (X = F (2), Cl (3), Br (4)). The most characteristic feature of all three solid-state structures of **2**−**4** is the coordination geometry of the central Si atom, which deviates significantly from the ideal tetrahedral form, as shown for the example of the fluoro derivative **2** (Figure 1a). For the Fe−Si−Fe angle, values of 125.3° (**2**), 125.4° (**3**), and 122.2° (**4**) are found, in accordance with Bent's rule, which predicts an enlargement of the angles including the two most electropositive silicon substituents. Consequently, the X−Si−X angles between the electronegative halogen substituents are considerably smaller (98.7°−99.3°).

In the solid state, **2**−**4** show C_2 symmetry. The view along one of the Fe−Si bonds, as shown in Figure 1b for the example of the bromo derivative **4**, reveals a distorted staggered conformation of the substituents in the bis(metallo)silanes **2**−**4**, with the following pairs adopting a mutually trans position: Cp/X, CO/X, and CO/Fe.

The Fe−Si bond distances in the bismetalated silanes **2**−**4** (2.2924−2.342 Å) are longer than those in comparable mono(ferrio)silanes $Cp(OC)_2Fe\text{-}SiR_3$ (2.20−2.29 Å).[11,27] This is probably the result of a much lower Fe−Si π-type back-bonding in the bis(ferrio)silanes, which is due to the competition of two electron-releasing $Cp(OC)_2Fe$ fragments on the same Si atom. Similar observations have been made for two other structurally characterized bis(ferrio)silanes: $[Cp(OC)_2Fe]_2SiH_2$ (2.34 Å)[12b] and $[Cp(OC)_2Fe]_2Si(H)OH$

(28) (a) Koe, J. R.; Powell, D. R.; Hayase, S.; Buffy, J. J.; West, R. *Angew. Chem.* **1998**, *110*, 1514−1515; *Angew. Chem., Int. Ed. Engl.* **1998**, *37*, 1441−1442. (b) Hengge, E.; Kovar, D. *Z. Anorg. Allg. Chem.* **1979**, *458*, 163−167.

(29) (a) Gaydon, A. G. *Dissociation Energies and Spectra of Diatomic Molecules*, 3rd ed.; Chapman and Hall: London, 1968. (b) Kondratiev, V. N. *Bond Dissociation Energies, Ionization Potentials and Electron Affinities*; Mauka Publishing House: Moscow, 1974.

Table 2. Selected Experimental Crystal Structure Data of $[Cp(OC)_2Fe]_2SiX_2$ with X = H (**1**), F (**2**), Cl (**3**), and Br **(4)**, in Comparison with the Calculated Structural Parameters of **1**−**5**

	1 (X = H)		**2** (X = F)		**3** (X = Cl)		**4** (X = Br)		
	exp[a]	calc[b]	exp	calc[b]	exp	calc[b]	exp	calc[b]	**5** (X = I), calc[c]
				Bond Lengths (pm)					
Si(1)−Fe(1)	234.2	234.0	229.24(4)	229.3	230.48(3)	231.7	230.21(19)	233.9	233.4
Si(1)−Fe(2)	234.0	237.2	229.55(4)	232.2	230.48(3)	234.6	230.21(19)	233.9	233.4
Si(1)−X(1)		151.7	164.12(8)	166.9	213.66(4)	217.2	231.8(2)	234.0	260.5
Si(1)−X(2)		151.3	163.23(9)	166.9	213.66(4)	216.5	231.8(2)	234.0	260.5
Fe(1)−C(1A)	174.2(5)	174.0	175.65(16)	174.5	175.78(15)	175.1	175.8(10)	175.3	175.4
Fe(1)−C(1B)	175.5(4)	174.1	175.34(15)	174.4	175.12(15)	174.8	173.9(9)	174.0	174.1
C(1A)−O(1A)	113.6(5)	116.4	115.21(19)	116.1	114.23(18)	115.9	115.6(10)	115.9	115.8
C(1B)−O(1B)	114.5(7)	116.4	115.28(19)	116.2	114.64(18)	116.1	116.0(9)	116.5	116.5
Fe(1)−Z(Cp)	172.3(6)		172.9(1)		172.85(7)		173.3		
				Bond Angles (degrees)					
X(2)−Si(1)−X(1)	104.00	102.6	99.22(5)	101.9	99.31(3)	101.2	98.74(12)	100.3	101.0
Fe(1)−Si(1)−Fe(2)	123.48(6)	124.8	125.269(18)	126.8	125.44(2)	125.8	122.16(14)	122.6	122.8
Fe(1)−Si(1)−X(1)	103.78	107.6	108.45(3)	107.9	108.606(11)	107.4	108.25(5)	105.8	105.2
C(1B)−Fe(1)−C(1A)	94.0(2)	92.9	95.99(7)	93.0	93.80(7)	93.4	95.0(4)	93.9	94.1
O(1A)−C(1A)−Fe(1)	178.1(4)	177.6	177.16(14)	176.3	177.61(13)	175.3	178.3(7)	174.5	174.1
O(1B)−C(1B)−Fe(1)	178.1(5)	178.3	178.55(14)	177.3	178.10(14)	176.1	178.5(7)	175.9	175.5

[a] Data taken from a previous work.[12b] [b] Calculated with BPW91/6-311G(d); for **1** and **4**, symmetry transformations were used to generate equivalent atoms. #1 $-x+1,y,-z+1/2$ and #1 $-x+1,y,-z+1/2$. [c] Calculated using two basis sets: BPW91/3-21G(d) for the I atoms, and 6-311G(d) for the other atoms.

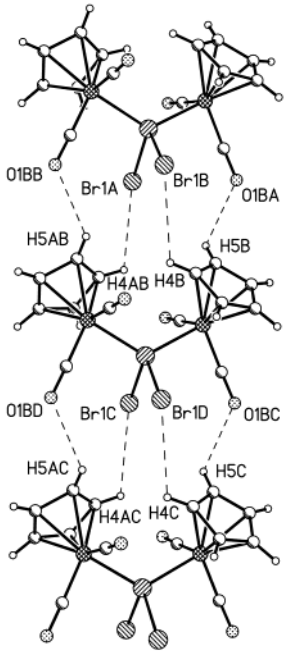

Figure 2. Hydrogen bridges Br1−H4 (3.20 Å) and O1B−H5 (2.56 Å) forming the chain structure of **4**.

(2.34 Å).[12a] It is also remarkable that the Fe−Si bond length in **2**−**4** is almost invariant, with respect to the type of halogen substituent on the silylene bridge, which means that no significant shortening of the Fe−Si bond is observed as the electronegativity of the substituents increases (Table 2).

As expected, all three halogen-substituted bis(ferrio)silanes **2**−**4** form intermolecular hydrogen bonds. In the case of $[Cp(OC)_2Fe]_2SiBr_2$ (**4**), a simple chain structure can be observed. The two strongest hydrogen bridges are found between the cyclopentadienyl hydrogens (H4, H5) and the Br or O1B atoms, respectively (Figure 2).

A similar arrangement is found for $[Cp(OC)_2Fe]_2SiCl_2$ (**3**), which involves the interaction of the Cl substituents with the H1 atom and the interaction of the carbonyl oxygen atom O1B with the H2 atom (Figure 3a). In addition, hydrogen bridges between the cyclopentadienyl hydrogen atom (H3) and the carbonyl groups (O1A) cross-link the chains of **3** in a plane (Figure 3b).

The solid-state structure of $[Cp(OC)_2Fe]_2SiF_2$ (**2**) is more complex. Two molecules are linked, via hydrogen bridges between a cyclopentadienyl hydrogen atom (H2) and a carbonyl oxygen atom (O2B), to a "dimer". Each dimer is connected to other dimers via strong hydrogen bridges between the fluoro substituents and the cyclopentadienyl hydrogen atoms (H3, H8), with each fluoro atom forming two hydrogen bonds to different molecules, resulting in a three-dimensional network (Figure 4).

The variety in the solid-state structures of **2**−**4** can be explained by the different strength of the H···X hydrogen bonds, which is greatest for **2**, because of the small and hard F atoms, and decreases in the following order: **2** ≫ **3** > **4**. This can also be deduced from the fact that, in the case of **2**, every F atom forms two hydrogen bonds to cyclopentadienyl hydrogen atoms. Recently, weak hydrogen bonding has also been studied by theoretical calculations.[30]

III. Vibrational Spectroscopy and DFT Calculations. The most-significant calculated and experimental fundamental vibrational modes, together with their Raman scattering activities, are summarized in Table 3. As one can notice, the calculated values agree well with the experimental data; however, some deviations were observed for the vibrations involving lone-pair atoms and the SiH_2 vibrations in **1**, for which anharmonicity is large. The results were then scaled to better approach the experimental spectra in these regions (Table 3). All other calculated wavenumbers were in very good agreement with the experimental values and should not be scaled. The best conformity between calculation and experimental data was observed for the cyclopentadienyl ring breathing and ν(CC) modes, for which the maximum deviations were only 4 and 6 cm^{-1}, respectively (Table 3).

(30) Calhorda, M. J. *Chem. Commun.* **2000**, 801−809.

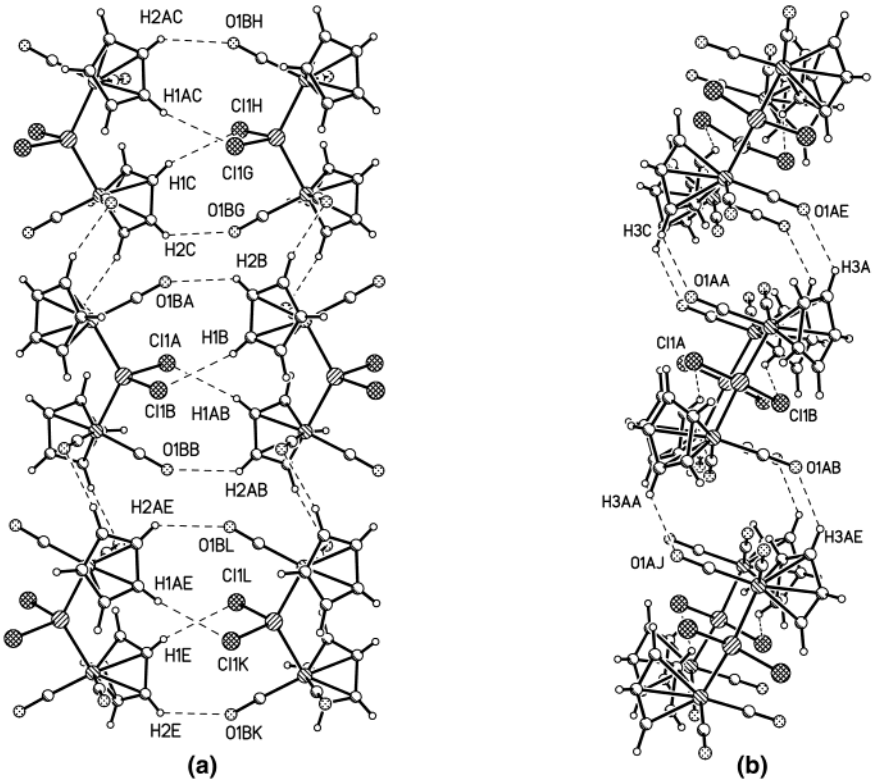

Figure 3. (a) View along the hydrogen-bridged chains of **3** with Cl1−H1 (2.88 Å) and O1B−H2 (2.58 Å). (b) View onto the cross-linked chains of **3** with O1A−H3 (2.56 Å).

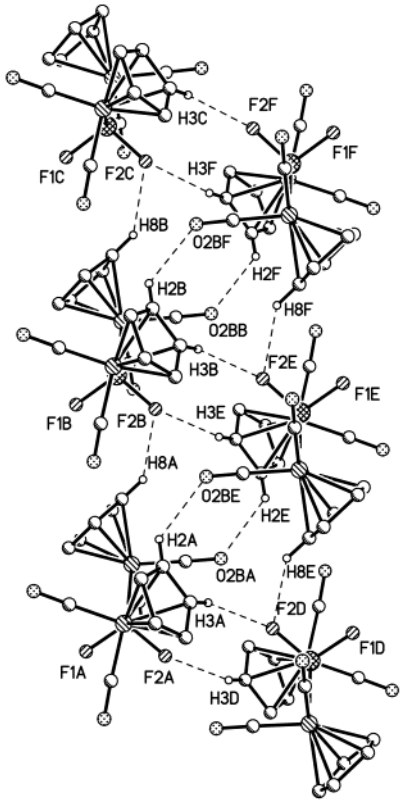

Figure 4. Segment of the three-dimensional network of **2**. Only the three strongest hydrogen bonds are shown: O2B−H2 (2.50 Å), F2−H3 (2.42 Å), and F2−H8 (2.42 Å).

The FT−Raman spectra of **1**−**4** in the CO spectral region are presented in Figure 5. Unfortunately, no Raman spectrum could be measured for $[Cp(OC)_2Fe]_2SiI_2$ (**5**), because of its decomposition under the laser light.

A closer examination of the 2100−1850 cm^{-1} spectral region in the FT−Raman spectra of **1**−**4** indicates the presence of two or more symmetrical and asymmetrical CO vibrational modes (Table 3, Figure 5). More exactly, **3** and **4** show only two ν(CO) vibrations, whereas more than two bands can be observed for **1** and **2** (Table 3, Figure 5). In the Raman spectrum of **1**, the bands at 2074 and 2043 cm^{-1} were assigned to symmetrical SiH stretching modes. For the other peaks at 2028, 1987, 1978, and 1928 cm^{-1}, the theoretical calculations and literature indicate CO stretching modes strongly mixed with symmetrical and asymmetrical SiH_2 stretching vibrations.[32,33] For **2**−**4**, these vibrations are "pure" CO stretchings and no other internal coordinates are involved.[32−37] As expected, the DFT calculations, which were performed without any symmetry restriction, led to more than two ν(CO) modes in each case (**1**−**5**) (Table 3). Taking into account that the X-ray structure determination indicated a

(31) Shillady, D. D.; Craig, J.; Rutan, S.; Rao, B. *Int. J. Quantum Chem.* **2002**, *90*, 1414−1420.
(32) Malisch, W.; Jehle, H.; Möller, S.; Thum, G.; Reising, J.; Gbureck, A.; Nagel, V.; Fickert, C.; Kiefer, W.; Nieger, M. *Eur. J. Inorg. Chem.* **1999**, 1597−1605.
(33) Nagel, V.; Fickert, C.; Hofmann, M.; Vögler, M.; Malisch, W.; Kiefer, W. *J. Mol. Struct.* **1999**, *480*−*481*, 511−514.
(34) (a) Jetz, W.; Graham, W. A. G. *J. Am. Chem. Soc.* **1967**, *89*, 2773−2775. (b) Malisch, W.; Kuhn, M. *Chem. Ber.* **1974**, *107*, 2835−2851. (c) Malisch, W.; Panster, P. *Chem. Ber.* **1975**, *108*, 2554−2573.
(35) Dalton, J.; Paul, I.; Stone, F. G. A. *J. Chem. Soc. A* **1969**, 2744−2749.
(36) Höfler, M.; Scheuren, J.; Spilker, D. *J. Org. Chem.* **1975**, *40*, 205−211.
(37) Thum, G.; Malisch, W. *J. Organomet. Chem.* **1984**, *264*, C5−C9.

Table 3. Selected Calculated and Experimental Fundamental Vibrational Wavenumbers (in cm^{-1}) for $[Cp(CO)_2Fe]_2SiX_2$ with X = H (**1**), F (**2**), Cl (**3**), Br (**4**), and I (**5**), Together with Their Tentative Assignments[a]

X = F (**2**)				X = Cl (**3**)				X = Br (**4**)				X = I (**5**)			X = H (**1**)				
IR	Raman	calc[b,c]	scal[e]	IR	Raman	calc[c]	scal[e]	IR	Raman	calc[c]	scal[e]	IR	calc[d]	scal[e]	IR	Raman	calc[c]	scal[e]	vibrational assignment
																2074 vw	2064	2028	$\nu_{sym.}$(SiH)
															2034	2043 vw	2042	2006	$\nu_{sym.}$(SiH)
2008	1999 ms	2025 (37.32)	1990	2012	2003 ms	2031	1996	2015	2006 ms	2027	1992	2016	2027	1992	2027	2028 ms	2007	1972	$\nu_{sym.}(SiH_2) + \nu_{sym.}(CO)$
1989	1983 w	2001 (27.40)	1966	1998		2006	1971	2000		2020	1985	2002	2021	1986	1986	1987 w	1994	1960	$\nu_{asym.}(SiH_2) + \nu_{asym.}(CO)$
very	1956 w	1982 (32.26)	1948			1989	1955	1962		1972	1938	1968	1974	1940	1967	1978 vw	1969	1934	$\nu_{sym.}(SiH_2) + \nu_{sym.}(CO)$
broad	1944 w														1921	1928 s	1949	1915	$\nu_{asym.}(SiH_2) + \nu_{asym.}(CO)$
1932	1931 ms	1956 (29.42)	1922	broad	1941 s	1960	1926	1945	1948 vs	1971	1937	1952	1973	1939	1913				$\nu_{asym.}(SiH_2) + \nu_{asym.}(CO)$
1434	1432 vw	1429 (10.62)	1404	1433	1432 vw	1430	1405	1431	1430 vw	1432	1407	1430	1431	1406	1432	1430 vw	1431	1406	ν(CC) + i.p. δ(CH)
1418	1419 vw	1414 (5.76)	1390	1418	1418 vw	1415	1391	1417	1419 vw	1415	1391	1415	1415	1391	1413	1414 vw	1414	1390	ν(CC) + i.p. δ(CH)
1367		1365 (2.40)	1341	1366		1366	1342	1366		1367	1343	1367	1367	1343	1366	1360 vw	1366	1342	ν(CC) + i.p. δ(CH)
	1117 s	1117 (101.21)	1098		1116 vs	1117	1098		1115 vs	1119	1100		1119	1100		1113 s	1116	1097	Cp ring breathing
1072	1070 vw	1063 (4.35)	1045	1063	1063 vw	1064	1046	1062	1064 vw	1062	1044	1062	1062	1045	1065	1062 w	1062	1044	i.p. δ(CH)
843		846 (0.61)	831	847	848 vw	848	833	848	849 vw	848	833	851	852	837	843	846 vw	845	830	$\omega(SiH_2)$ + o.p. δ(CH)
776		764 (0.55)	751																$\nu_{asym.}(SiF_2)$ + o.p. δ(CH)
747		726 (0.62)	713																$\nu_{sym.}(SiF_2)$ + o.p. δ(CH)
642		650 (3.66)	639	639		646	635	636		647	636	632	645	634	647	638 w	653	642	i.p. δ(FeCO) + $\tau(SiH_2)$ + o.p. δ(CH)
605		603 (0.48)	593	sh		602	592	602		605	595	597	604	594	604	601 vw	602	592	o.p. δ(FeCO) + $\tau(SiH_2)$ + o.p. δ(CH)
531	531 vw	535 (3.42)	526	521	526 w	527	518	519	525 sh	523	514	516	521	512	524	526 w	535	526	i.p., o.p. δ(FeCO)
520	521 vw	518 (0.96)	509		516 sh	518	509	515	519 w	512	503	508	509	500	516	513 sh	519	510	o.p. δ(CO)
467	464 vw	455 (1.28)	447	466	463 vw	461	453	462	458 w	455	447	460	452	444	465	463 vw	464	456	$\nu_{asym.}(SiCl_2) + \nu_{sym.}(SiBr_2) + \delta$(CO) + $\rho(SiH_2)$
sh		453 (2.37)	445	sh		452	444	sh		453	445	sh	451	443			452	444	$\nu_{sym.}(SiCl_2) + \delta$(CO) + $\rho(SiH_2) + \delta(SiX_2)$
435		435 (0.82)	427	425		428	421					420	398	391			434	426	
	426 vw	430 (0.92)	423		426 vw	419	412		394 vw	384	377		384	377					o.p. δ(CH) + o.p. δ(FeCO) + $\omega(SiF_2) + \nu_{sym.}(SiCl_2)$
	398 vw	390 (6.69)	383		387 w	384	377		374 vs	376	369		374	368			397	390	$\nu_{asym.}$(FeCp) + $\nu_{sym.}(SiBr_2) + \omega(SiH_2)$ + o.p. δ(FeCO)
		385 (7.68)	378			379	372			376	370		370			389 m	390	383	$\nu_{asym.}$(SiFeCp) + $\rho(SiH_2) + \omega(SiX_2)$ + o.p. δ(FeCO)
	376 vs	370 (5.88)	364		369 vs	367	361		353 m	358	352		358	352		365 s	364	358	$\nu_{sym.}$(FeCp) + $_{asym.}(SiBr_2)$ + i.p., o.p. δ(FeCO)
	350 ms	367 (23.60)	361			350	344			344	338		342	336					$\nu_{sym.}$(SiFeCp) + $\omega(SiF_2)$ + o.p. δ(FeCO)
													325	319		328 vw	334	328	$\nu_{sym.}(SiI_2) + \omega(SiH_2) + \nu_{sym.}$(FeCp) + i.p., o.p. δ(FeCO)
													321	315					$\nu_{asym.}(SiI_2) + \nu_{asym.}$(FeCp) + i.p., o.p. δ(FeCO)
																276 vs	276	271	$\delta_{sym.}$(FeCp) + i.p. $\delta(SiH_2)$ + o.p. δ(FeCO)
	242 vw	228 (1.56)	224		245 vs	238	234												$\delta_{asym.}$(FeCp) + $\gamma(SiCl_2) + \omega(SiF_2)$ + o.p. δ(FeCO)
	224 vs	215 (19.19)	211																i.p. $\delta(SiF_2) + _{sym.}$(FeCp) + o.p. δ(FeCO)
									204 s	191	188								$\nu_{sym.}(SiBr_2) + \delta_{asym.}$(SiFeCp) + o.p. δ(FeCO)

[a] Wavenumbers are given in units of cm^{-1}. Legend for abbreviations: vw, very weak; w, weak; m, medium; ms, medium strong; s, strong; vs, very strong; sh, shoulder; sym., symmetrical; asym., asymmetrical; i.p., in-plane; o.p., out-of-plane; ν, stretching; δ, bending; ω, wagging; τ, twisting; ρ, rocking; and γ, scissoring. [b] Calculated Raman scattering activities, shown in parentheses, are given in units of $Å^4$/amu. [c] Calculated with BPW91/6-311G(d). [d] Calculated using two basis sets: BPW91/3-21G(d) for the I atoms, and 6-311G(d) for the other atoms. [e] Scaled by 0.9827, according to the value proposed by Shillady et al.[31]

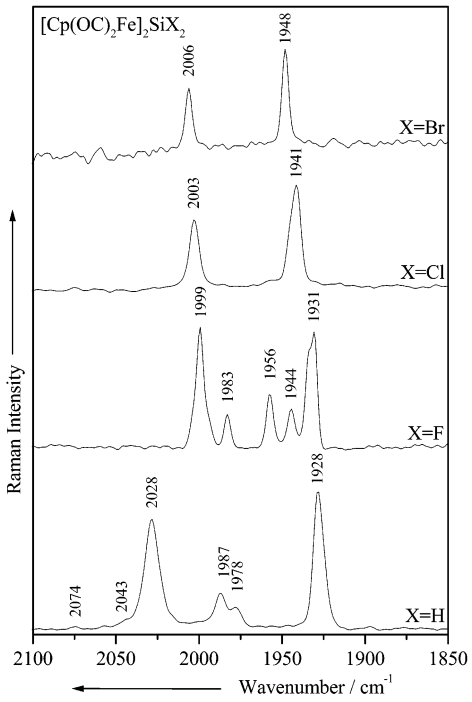

Figure 5. FT−Raman spectra of **1**−**4** in the CO spectral region. Excitation line is located at 1064 nm.

C_2 symmetry for all complexes, we believe that the appearance of more than two bands in the CO spectral region of **2** (1999, 1983, 1956, 1944, and 1931 cm^{-1}) is mostly due to the existence of different conformers, as previously reported for similar compounds.[34]

For complexes **2**−**4**, the ν(CO) vibration is coupled only with other ν(CO) vibrations; therefore, the wavenumber shift can be taken as a direct measure of bond strength. As one can notice (Figure 5, Table 3), the sequential replacement of the H atoms with either F, Cl, or Br atoms on the Si atom causes the ν(CO) values to increase. Furthermore, the magnitude of this effect depends on the substituents in the following order: F < Cl < Br (i.e., 1999, 2003, 2006 cm^{-1} and 1931, 1941, 1948 cm^{-1}). The same trend was observed in the IR spectra and confirmed by the DFT calculations (F < Cl < Br ≤ I), although the experimental values differ in this case by almost 30 cm^{-1} from the experimental data (Table 3). However, when scaled by 0.9827 in this spectral region,[31] the calculated CO stretching modes come very close to the experimental values (Table 3). This is a very surprising result, because it is contrary to the tendency observed for other homologous silyl complexes $(OC)L_nM\text{-}SiR_3$,[11] where the ν(CO) values decreased as the electronegativity of the silyl substituent decreased.

This unexpected shift of the carbonyl stretching mode to higher wavenumbers could be explained by an increase of the electron density on the metal available for d-π-type back-bonding to the π*(CO) orbitals. The NPA (Table 4) actually reveals that the Fe atoms in **1**−**5** are positively charged, with the lowest formal charge being found for the fluorine derivative **2** (+0.698) and significantly higher charges being observed for the other halogen derivatives **3**−**5**. Despite the undoubtedly higher electronegativity of the SiF_2 unit, the Fe atom in **2** still bears the highest electron density. The reasons for these observations can be rationalized assuming a π-type bonding from the nonbonding halogen valence electrons to the unoccupied d(Si) or σ*(Fe−Si) orbitals. Such a π-type overlap is more efficient for smaller orbitals (e.g., in F) than for the more diffuse orbitals of the larger halogen substituents and might therefore overcompensate the opposite ionic contributions to the Fe−Si bond.

Table 4. Partial Charges[a] Situated on Selected Atoms of $[Cp(OC)_2Fe]_2SiX_2$ with X = H, F, Cl, Br, and I (**1**−**5**), Determined by the Natural Population Analysis

atom	**1**[b]	**2**[b]	**3**[b]	**4**[b]	**5**[c]
X	−0.063	−0.402	−0.336	−0.265	−0.128
Si	−0.076	+0.676	+0.167	+0.100	−0.330
Fe	+0.740	+0.698	+0.767	+0.766	+0.805
C	−0.026	−0.036	−0.020	+0.011	+0.034
O	−0.196	−0.186	−0.175	−0.162	−0.159

[a] Given in units of e. [b] Calculated with BPW91/6-311G(d). [c] Calculated using two basis sets: BPW91/3-21G(d) for the I atoms, and 6-311G(d) for the other atoms.

For a better understanding of the π-type bonding from the nonbonding halogen valence electrons to the unoccupied d(Si) or σ*(Fe−Si) orbitals, we performed an NBO analysis for quantitative information regarding these second-order interactions. Table 5 shows the occupancy of the lone-pair orbitals n_x at the halogen atoms and that of the σ*(Fe−Si) orbitals. As one can notice, the ionic contribution decreases in the order F > Cl > Br > I, as indicated by the presence of four lone-pair orbitals of the fluoro and chloro derivatives (**2** and **3**); the most electronegative compound **2** presents a higher occupancy. As we have already mentioned, the NPA analysis indicates that the Fe atom in **2** has the highest electron density, in comparison with **3**−**5** (Table 4), which is further substantiated by the NBO results (Table 5) that show a decrease in the population of the σ_1*(Fe−Si) orbitals when going from **2** to **5**. The NBO analysis reveals that σ_1*(Fe−Si) orbitals are a mixture of Fe- and Si-centered hybrids, which have sd form at the Fe atom and sp form at the Si atom. In contrast to this, σ_2*(Fe−Si) orbitals have almost pure Si character (Table 5). Moreover, a lone-pair orbital—composed of a hybrid of a high p-character and an occupancy of 0.63 and 0.59 e, respectively (Table 5)—at the Si atom was detected only for **2** and **3**. We would like to mention that the possible discrepancies in the calculated values of complex **5** (in comparison with the other complexes, **2**−**4**) may be caused by the different basis set employed in this case for the halogen atom (3-21G(d) for the I atoms and 6-311G(d) for the other atoms).

Table 6 presents the strengths of the perturbative donor−acceptor interactions, which involve occupied and formally unoccupied NBOs. A closer examination of the stabilization energies in Table 6 reveals stronger π-type back-bonding for **2** and **3**, showing slightly higher energy values for the chlorine compound **3** (417.35 kJ/mol) and very small values for the other derivatives (**4** and **5**). However, for the σ_1*(Fe−Si) orbital, the highest stabilization energy (120.88 kJ/mol) was found in the fluorine compound **2**. In addition, in the case of the fluoro derivative **2**, we also observed a strong $n_{Si} \rightarrow \sigma$*(Fe−Si) interaction (929.27 kJ/mol) that should lead

Table 5. Orbital Occupancy (e) and Contributions of Atomic Orbitals (%) for $[Cp(OC)_2Fe]_2SiX_2$ with X = F, Cl, Br, and I (**2**−**5**)

	2[a]	**3**[a]	**4**[a]	**5**[b]
σ_1*(Fe−Si)	0.46858 e ($sd^{1.87}$, $sp^{0.23}$)	0.40984/0.38207 e ($sd^{1.93}$, $sp^{1.30}$)	0.38570/0.36686 e ($sd^{1.81}$, $sp^{2.25}$)	0.34184 e ($sd^{1.92}$, $sp^{1.21}$)
Fe	52.30%	56.56%	55.78%	47.25%
Si	47.70%	43.44%	44.22%	52.75%
σ_2*(Fe−Si)	0.54904/0.38657 e (d, p)	0.46016 e (d, p)		0.48267/0.90064 e (d, p)
Fe	4.84%	4.83%		4.24%
Si	95.16%	95.17%		95.76%
n_{Si}	0.62590 e ($sp^{5.62}$)	0.58662 e ($sp^{7.43}$)		
n_x (1)	1.97890 e ($sp^{0.67}$)	1.97684 e ($sp^{0.35}$)	1.97774 e ($sp^{0.27}$)	1.98099 e ($sp^{0.17}$)
n_x (2)	1.93219 e (p)	1.94419 e (p)	1.93461 e (p)	1.93833 e (p)
n_x (3)	1.92907 e (p)	1.93430 e (p)	1.92902 e (p)	1.93250 e (p)
n_x (4)	1.79020 e ($sp^{1.48}$)	1.57587 e ($sp^{2.86}$)		

[a] Calculated with BPW91/6-311G(d). [b] Calculated using two basis sets: BPW91/3-21G(d) for the I atoms, and 6-311G(d) for the other atoms.

Table 6. Results of the NBO Analysis for $[Cp(OC)_2Fe]_2SiX_2$ with X = H (**1**), F (**2**), Cl (**3**), Br (**4**), and I (**5**)

	2[a]	**3**[a]	**4**[a]	**5**[b]
	$n_x \rightarrow \sigma_2$*(Fe−Si)			
$E(2)$ (kJ/mol)[c]	271.29	417.35		72.59
$\epsilon(j) - \epsilon(i)$ (a.u.)	0.74	0.38		1.11
$F(i, j)$ (a.u.)	0.205	0.174		0.141
	$n_x \rightarrow \sigma_2$*(Fe−Si)			
$E(2)$ (kJ/mol)[c]	92.88	106.60		73.97
$\epsilon(j) - \epsilon(i)$ (a.u.)	0.81	0.75		0.05
$F(i, j)$ (a.u.)	0.133	0.140		0.031
	$n_x \rightarrow \sigma_1$*(Fe−Si)			
$E(2)$ (kJ/mol)[c]	120.88	21.51	25.94	2.26
$\epsilon(j) - \epsilon(i)$ (a.u.)	0.80	0.56	0.24	0.36
$F(i, j)$ (a.u.)	0.146	0.049	0.036	0.013
	$n_{Si} \rightarrow \sigma_2$*(Fe−Si)			
$E(2)$ (kJ/mol)	929.27			
$\epsilon(j) - \epsilon(i)$ (a.u.)	0.01			
$F(i, j)$ (a.u.)	0.059			
	$n_{Si} \rightarrow \sigma_1$*(Fe−Si)			
$E(2)$ (kJ/mol)	245.60	38.28		
$\epsilon(j) - \epsilon(i)$ (a.u.)	0.12	0.20		
$F(i, j)$ (a.u.)	0.101	0.054		

[a] Calculated with BPW91/6-311G(d). [b] Calculated with BPW91/3-21G(d) for the I atoms and 6-311G(d) for the other atoms. [c] For each lone pair, only the donor−acceptor interactions with the highest $E(2)$ values have been taken into consideration. $E(2) = q_i[F(i,j)^2/(\epsilon_j - \epsilon_i)]$, where $E(2)$ is the second-order perturbational energy stabilization. $F(i,j)$ is the Fock matrix element between an occupied orbital i and an unoccupied orbital j. $F(i,j)$ is proportional to the overlap between orbitals i and j. $\epsilon(j) - \epsilon(i)$ is the energy difference between orbitals i and j, and q_i is the occupancy of donor orbital i. Thus, NBO analysis can be used to examine conjugation effects in π-conjugated systems quantitatively.[23−26]

to a significant π-stabilization of **2**. This effect is negligible for the other three compounds (**3**−**5**).

The introduction of halogen atoms at the Si site can be monitored in a straightforward manner by the disappearance of the SiH stretching modes of **1** at 2074 and 2043 cm^{-1} and the simultaneous formation of new bands in the IR and Raman spectra of **2**−**5**, which is characteristic to the symmetrical and asymmetrical SiX_2 stretching vibrations (Table 3, Figures 5 and 6). One can notice that, upon substitution of the H atom with either a F, Br, or Cl atom on the Si atom, the $\nu(SiX_2)$ modes are shifted significantly to lower wavenumbers, because of mass effects. Moreover, they strongly mix with other vibrations. Consequently, the wavenumber shift cannot give us any further information.

Unfortunately, the very interesting symmetrical and asymmetrical Fe−Si stretching modes can be observed only in the Raman spectrum of **1**, as a medium signal at 390 cm^{-1}

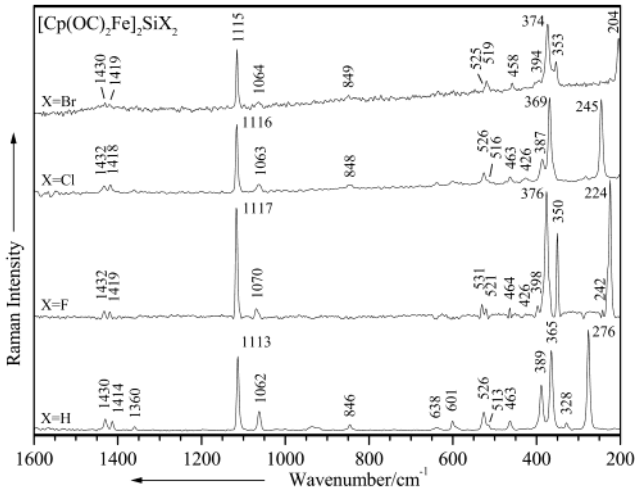

Figure 6. FT−Raman spectra of **1**−**4** between wavenumbers of 1600 and 200 cm^{-1}. Excitation line is located at 1064 nm.

(symmetrical ν(Fe−Si)), and in that of **2**, as a medium-strong peak at 350 cm^{-1} (asymmetrical ν(Fe−Si)) (Table 3, Figure 6). The visualization of these vibrations shows a strong coupling with the symmetrical and asymmetrical Fe−Cp stretching mode, respectively. Hence, these motions should be better ascribed to a symmetrical and asymmetrical ν(SiFeCp) mode (Table 3). Nevertheless, the calculated values are consistent with the assumed weakening of the Fe−Si bond, because of the π-type bonding of the nonbonding halogen valence electrons with the unoccupied d(Si) or σ*-(Fe−Si) orbitals. More exactly, the asymmetrical ν(SiFeCp) modes of **2**−**5** were found to decrease in the order F, Cl, Br, and I (385, 379, 376, and 370 cm^{-1}). A similar tendency is present in the symmetrical ν(SiFeCp) modes, which were theoretically determined at 361, 350, 344, and 342 cm^{-1} in **2**−**5**.

Because of its relative intensity and characteristic wavenumber (1110 ± 10 cm^{-1}), the ring breathing mode of the cyclopentadienyl ring can be considered to be the most evident vibration of the group (Figure 6). As also indicated by the calculated harmonic vibrational wavenumbers, the cyclopentadienyl ring breathing mode of **1**−**5** does not change substantially upon the substitution of X (Table 3, Figure 6). A similar behavior is present in the CC stretching vibrations of the cyclopentadienyl ring, which strongly couple with the CH in-plane deformations and give rise to the peaks at 1435−1360 cm^{-1} in the Raman spectra of **1**−**5** (Figure

6, Table 3). So, we can conclude that the changes in the electronic density on the metal have no influence on these bonds.

Conclusion

This paper describes the synthesis and characterization of bis(ferrio)silanes of the type $[Cp(OC)_2Fe]_2SiX_2$ (X = F, Cl, Br, I). The availability of a full series of homologous compounds gave us the opportunity to perform a systematic study of the bonding situation in these complexes using X-ray crystallography, vibrational spectroscopy, and density functional theory calculations. In this context, the nature of the Fe−Si bond and the influence of the various substituents H, F, Cl, Br, and I on the silylene bridge seemed to be of particular interest.

The Fe−Si distance can be taken as a measure of the bond strength in these complexes. The experimental and calculated Fe−Si bond distances in **1**−**5** are generally larger than those in other mono(ferrio)silanes $Cp(OC)_2Fe\text{-}SiR_3$; however, significant variation of the bond length, relative to the type of halogen substituent, could not be observed. The calculated Fe−Si stretching vibrations predict an increase in wavenumber and, hence, bond strength, in the following order: I < Br < Cl < F. This is a typical consequence of the ionic bonding contribution between the iron fragment and the silylene unit SiX_2, with increasing electronegativity of X.

A remarkable result was found for the wavenumbers of the CO stretching modes, which are increasing in the following order: F < Cl < Br ≤ I. It must be assumed that the π-type back-bonding of the nonbonding orbitals of the halogen substituent X into unoccupied σ^*(Fe−Si) orbitals is responsible for this effect. All observed structural and vibrational properties are clearly indicating a strong electron-donating influence of the iron fragments on the silylene unit. This transition-metal effect previously has been invoked to rationalize some unusual characteristics and reactivities of mono- and bis(ferrio)silanes, e.g., the stabilization of Si(OH) units toward condensation or the activation of SiH moieties for halogenation and oxygenation reactions.

Further studies concerning the reactivity of this interesting class of compounds are currently in progress and are focused on the preparation of unusual metal−silicon species, such as bismetalated silylenes $[Cp(OC)_2Fe]_2Si$ and silanones $[Cp(OC)_2Fe]_2Si{=}O$.

Acknowledgment. We gratefully acknowledge financial support from the Deutsche Forschungsgemeinschaft (Schwerpunktprogramm "Spezifische Phänomene in der Siliciumchemie"; SFB 347 "Selektive Reaktionen metallaktivierter Moleküle"), as well as support from the Fonds der Chemischen Industrie.

Supporting Information Available: X-ray crystallographic files for **2**−**4** in CIF format. This material is available free of charge via the Internet at http://pubs.acs.org.

IC026138V